

Supporting Information

First-Principles Insights into Dopant-Vacancy Interactions in Acceptor-Doped Perovskites

Yoshikazu Kikuchi,¹ Takaya Fujisaki,² Tatsumi Ishihara,^{1,3}

John Kilner,^{3,4} Aleksandar Staykov^{1,3}*

¹ Faculty of Engineering Department of Applied Chemistry, Kyushu University, 744
Motooka, Nishi-ku, Fukuoka 819-0395, Japan

² Faculty of Materials for Energy, Shimane University, 1060, Nishikawatsu, Matsue, Shimane
690-0823, Japan

³ International Institute for Carbon-neutral Energy Research (WPI-I2CNER), Kyushu
University, 744 Motooka, Nishi-ku, Fukuoka 819-0395, Japan

⁴ Department of Materials, Imperial College London, London SW7 2AZ, U.K.

* Corresponding author alex@i2cner.kyushu-u.ac.jp

Table S1: Host structures and the dopant cations.

Host material	Dopant (A-site doping)		Dopant (B-site doping)	
	Group 1	Group 2	Group 1	Group 2
LaAlO ₃	Sr ²⁺	Ba ²⁺	Mg ²⁺	Cu ²⁺
LaGaO ₃	Sr ²⁺	Ba ²⁺	Mg ²⁺	Cu ²⁺
SrTiO ₃	Na ⁺	K ⁺	Sc ³⁺	Fe ³⁺

Table S2: Initial phase, supercell scaling factor, and k-point grid used for structural relaxation of each host material

Host material	Phase	repetition	k-point grid
LaAlO ₃ (800 K)	Pm3_m	2*2*4	4*4*2
LaAlO ₃ (0 K)	R3_c	※	3*3*4
LaGaO ₃ (800 K)	R3_c	※	4*4*2
LaGaO ₃ (0 K)	Pnma	2*2*1	3*3*4
SrTiO ₃ (800 K)	Pm3_m	2*2*4	4*4*2
SrTiO ₃ (0 K)	I4/mcm	2*2*1	3*3*4

Figure S1: Comparison of trends for STO with 80 and 320 atoms in the supercell and Sc without DFT+U correction and 3.0 eV Hubbard correction.

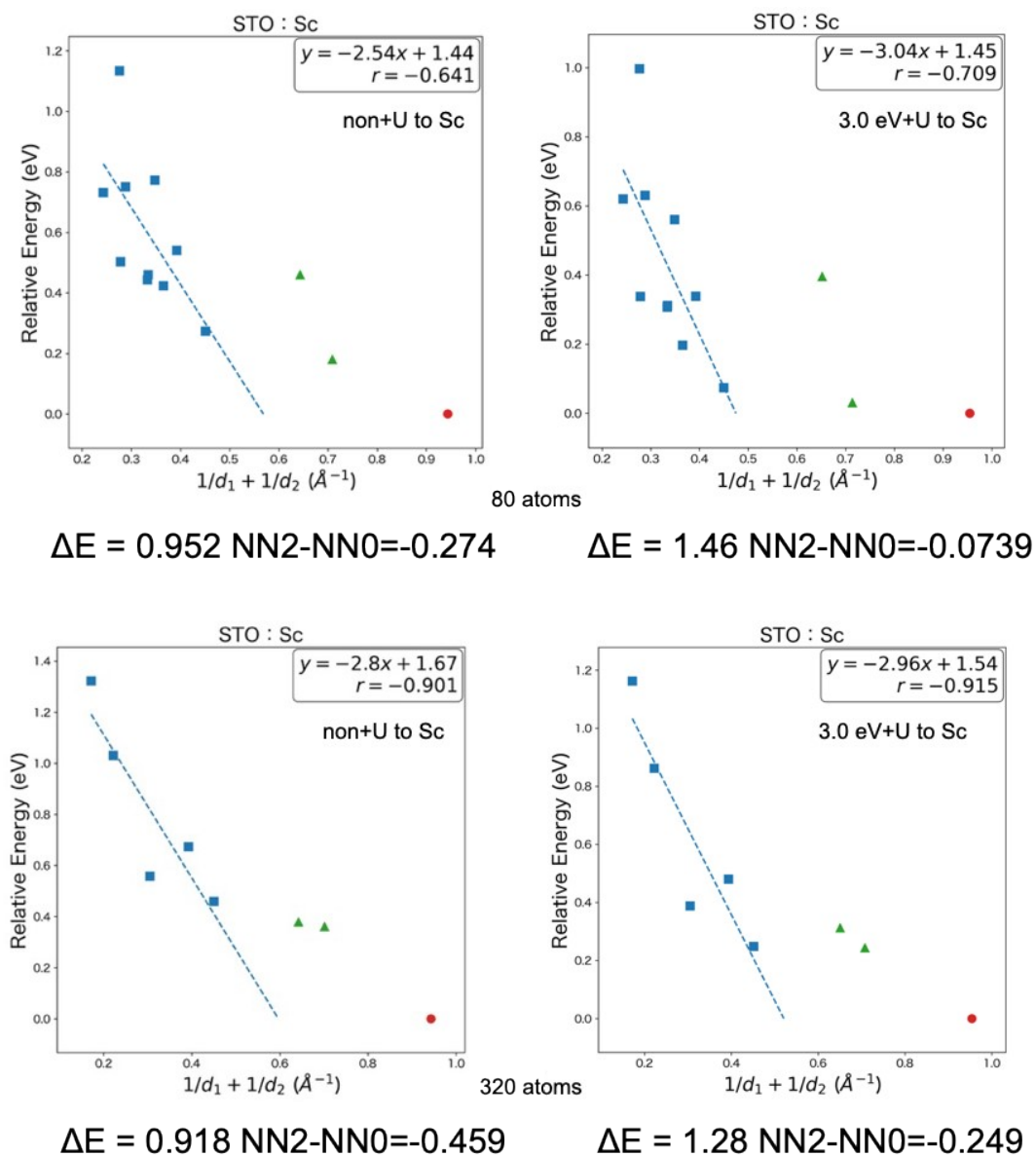
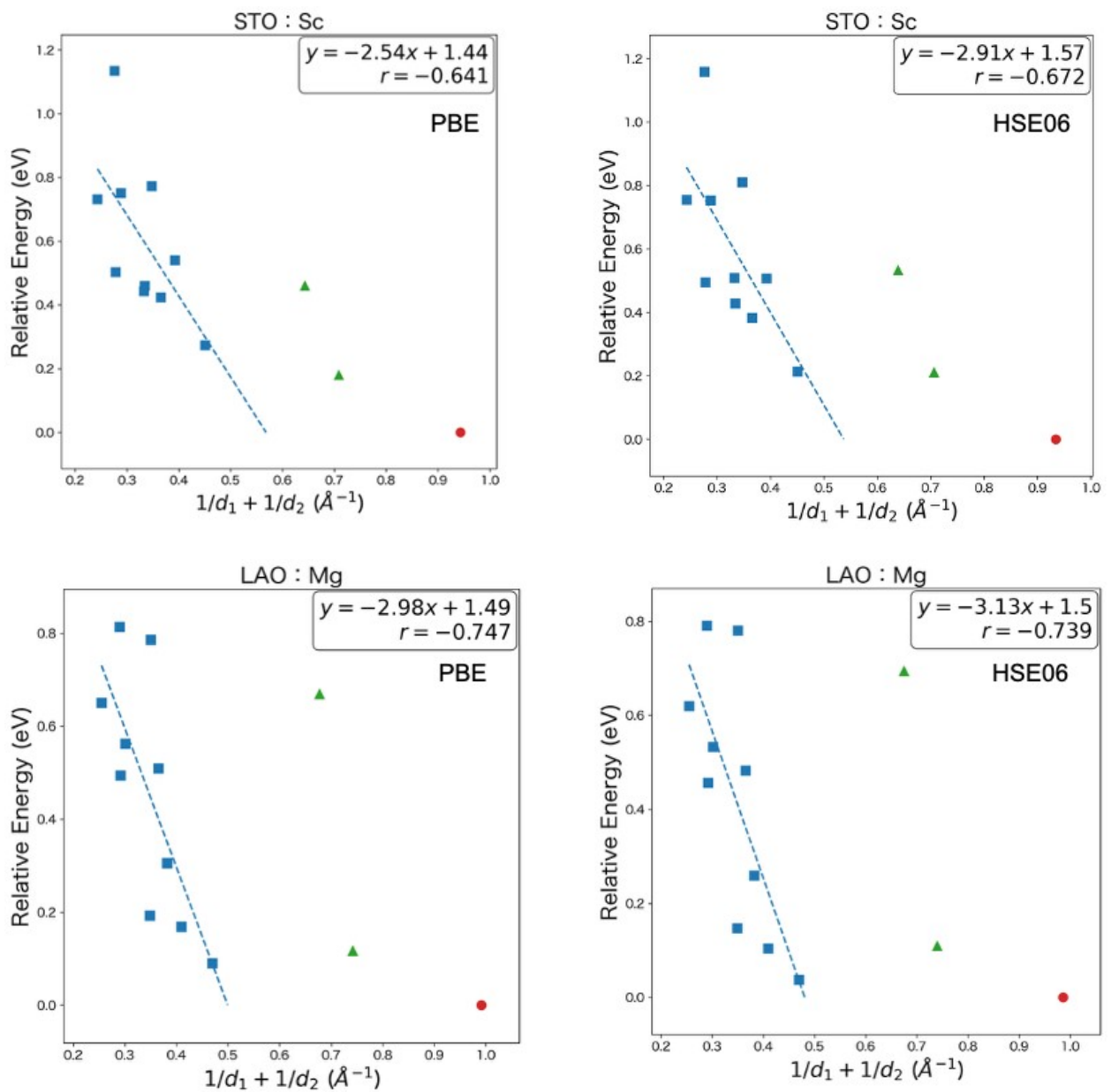
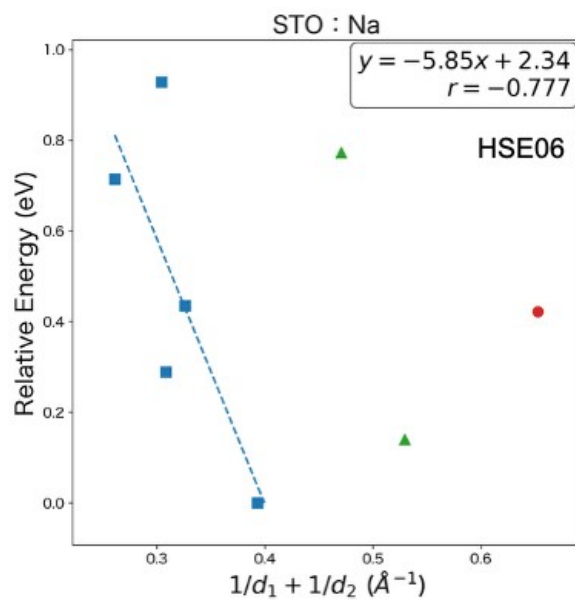
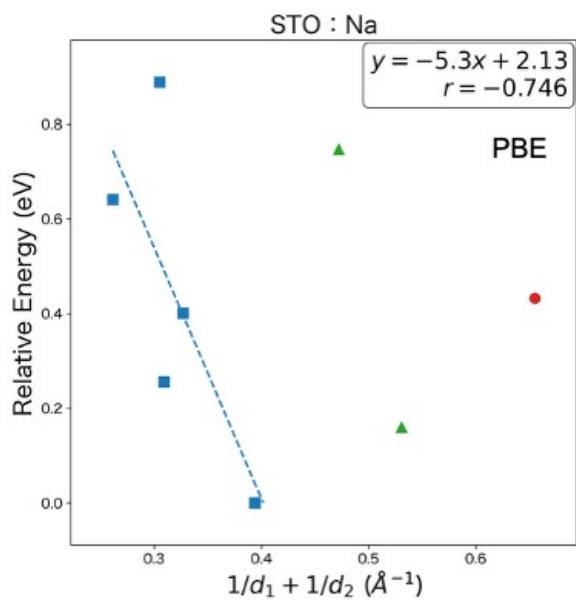
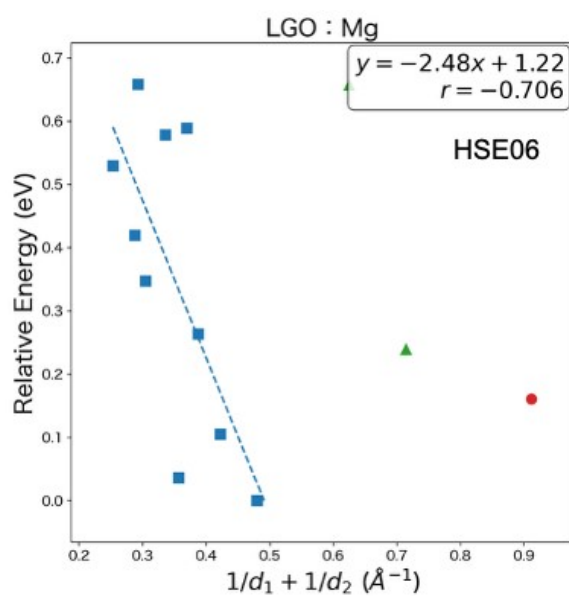
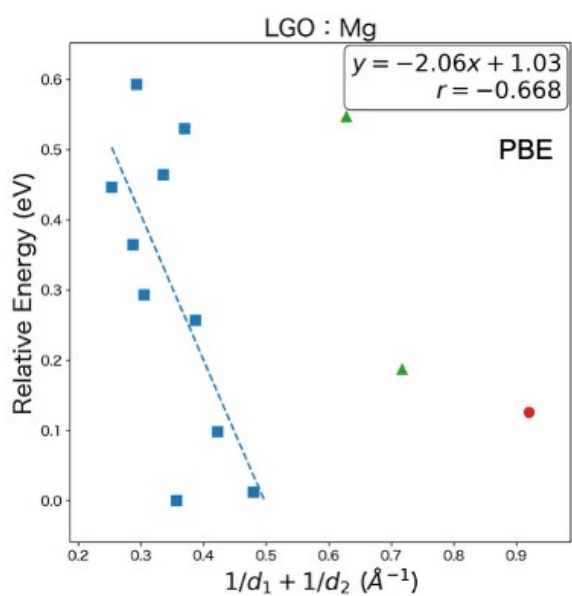
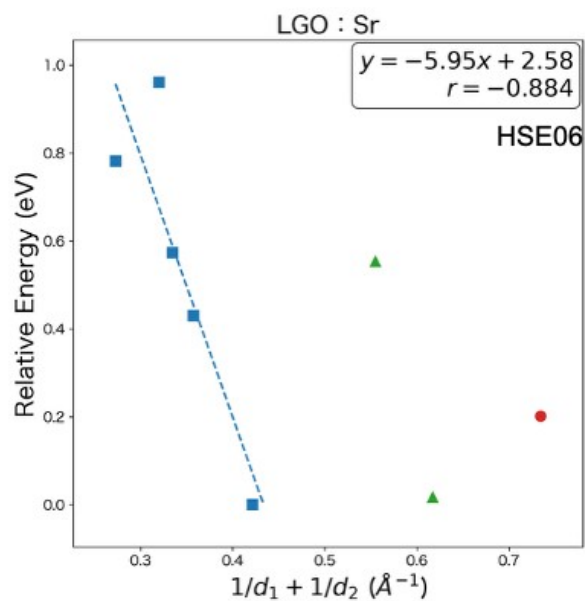
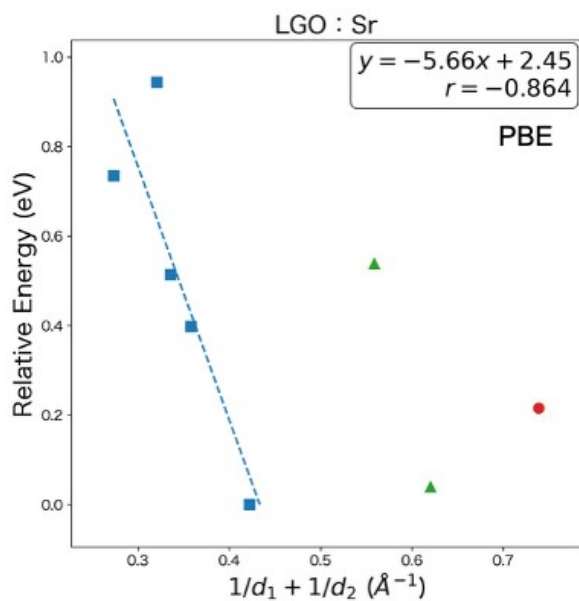


Figure S2: Comparison of trends for various lattices with 80 atoms in the supercell and between PBE (PBE+U where applicable) and HSE06.



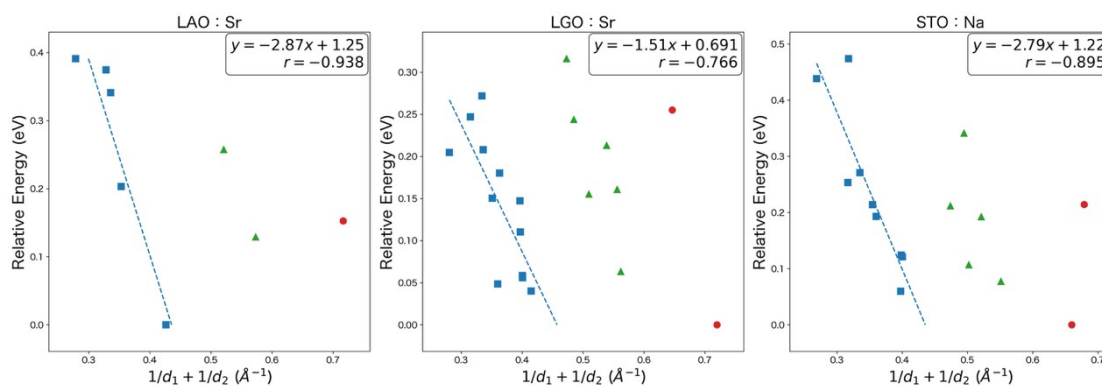




0 temperature Stable Phases with 80 atoms in the supercell

Figure S3 shows the relative energies of vacancy configurations plotted as functions of the Coulomb metric for Sr- or Mg-doped LaAlO₃, Sr- or Mg-doped LaGaO₃, and Na- or Sc-doped SrTiO₃ in the 80-atom supercells of the 0 K stable phase. For A-site-doped LGO and STO, two distinct NN2 configurations are present, corresponding to axial and equatorial arrangements.

a



b

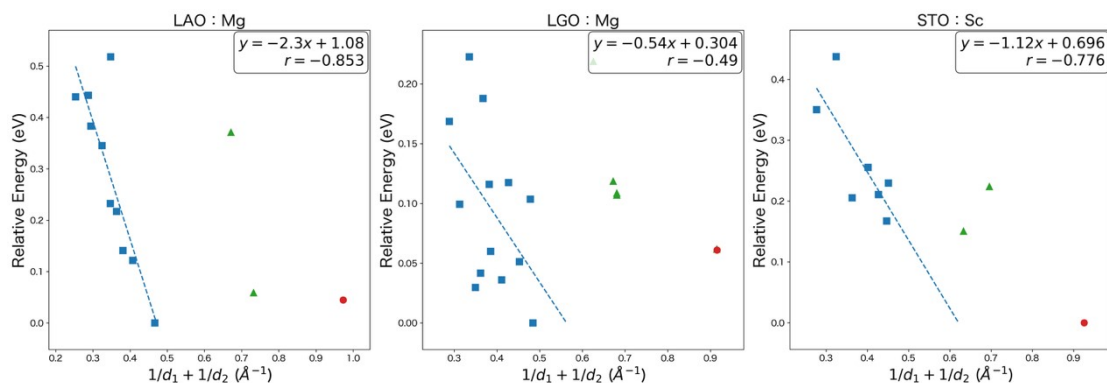


Figure S3. Relative energies of vacancy configurations plotted as functions of the Coulomb metric ($1/d_1 + 1/d_2$) for the 80-atom supercells constructed from the most stable 0 K phase. (a) A-site doping; (b) B-site doping. Blue squares, green triangles, and red circles correspond to NN0, NN1, and NN2 configurations, respectively. The dotted line represents a linear fit to the NN0 data. The fitting equation and the corresponding correlation coefficient (r) are given in the upper-right corner of each panel.

Overall, the results exhibit trends similar to those obtained for the 800 K stable phase, supporting the physical validity of the constrained structural relaxations employed in this work. For Mg-doped LaGaO₃, however, the linear fit for the NN0 configurations is substantially weaker ($|r| = -0.49$). We attribute this behavior primarily to the strong dependence of vacancy energies on whether the vacancy occupies an axial or equatorial position. Consistent with this interpretation, Gambino et al. reported a pronounced energy difference between axial and equatorial vacancy configurations in Mg-doped LGO.